JAERI-M
86-170

# ABLATION OF HYDROGEN ICE PELLET IN JT-60 PLASMA

October 1986

Toshio HIRAYAMA, Kimio YAMADA,* Seio SENGOKU
and Masayuki NAGAMI

日本原子力研究所
Japan Atomic Energy Research Institute

JAERI-Mレポートは，日本原子力研究所が不定期に公刊している研究報告書です。
入手の問合わせは，日本原子力研究所技術情報部情報資料課（〒319-11茨城県那珂郡東海村）あて，お申しこしください。なお，このほかに財団法人原子力弘済会資料センター（〒319-11 茨城県那珂郡東海村日本原子力研究所内）で複写による実費頒布をおこなっております。

JAERI-M reports are issued irregularly.
Inquiries about availability of the reports should be addressed to Information Division Department of Technical Information, Japan Atomic Energy Research Institute, Tokai-mura, Naka-gun, Ibaraki-ken 319-11, Japan.



編集兼発行　日本原子力研究所
印　　刷　いばらき印刷㈱

JAERI-M 86-170

# ABLATION OF HYDROGEN ICE PELLET IN JT-60 PLASMA

Toshio HIRAYAMA, Kimio YAMADA*, Seio SENGOKU +
and Masayuki NAGAMI

Department of Large Tokamak Research
Naka Fusion Research Establishment
Japan Atomic Energy Research Institute
Naka-machi, Naka-gun, Ibaraki-ken

(Received October 15, 1986)

Ablation of hydrogen ice pellet in the JT-60 plasma was calculated by ORNL pellet ablation code, which employs a neutral gas shielding model. An optimum scheme to produce central peaked $n_e$ profile of $n_e(0)=2\times10^{-3}$ and $n_e(0)/\langle n_e\rangle$ ~ 3 in the ohmic discharge appears to be a pellet injection with the pellet size of 3.4 mm diameter and velocity of 2 km/s. Under the assumption of electron heat diffusivity $\chi_e=2\times10^{19}/n_e$ ($m^2/s$), the 1-D tokamak code (LIBRARY) predicts ~30% increment of fusion multiplication (Q) for pellet fueled peaked density profile compared with gas fueled discharge.

Keywords: JT-60, Tokamak, Plasma, Pellet, Ablation, Fusion Power Multiplication, LIBRARY

---

+ Department of Thermonuclear Fusion Research

* On leave from Energy Research Laboratory, Hitachi, Ltd.

# JT−60 プラズマにおける水素氷ペレットの蒸発

日本原子力研究所那珂研究所臨界プラズマ研究部
平山俊雄・山田喜美雄*・仙石盛男†・永見正幸

（1986 年 10 月 15 日受理）

JT−60 のプラズマに入射する水素氷ペレットの蒸発について，中性ガスしゃへいモデルを用いた ORNL のペレット蒸発計算コードを使い，ペレット入射のための条件を明らかにすると共に，追加熱用ターゲットプラズマ生成の最適条件を示した。中心密度 $n_e(0)=2\times10^{20}m^{-3}$，及び $n_e(0)/\langle n_e\rangle\sim3$ となる中心ピークの密度分布を，直径 3.4 mm のペレットを 2 km/s の速さでオーミック・プラズマに入射することにより，得ることができる。電子の熱伝導係数 $\chi_e=2\times10^{19}/n_e(m^2/s)$ を仮定した一次元トカマクコード（LIBRART）の計算より，ガス補給による平坦密度分布のプラズマに較べて，ペレット入射による急峻密度分布のプラズマにおいて，核融合増倍率 Q が約 30 %改善されることを示す。

那珂研究所：〒 311−02 茨城県那珂郡那珂町大字向山 801−1
† 核融合研究部・プラズマ実験室
* 外来研究員：日立製作所エネルギ研究所

Contents

# 目　　次

## 1. Introduction

The recent Experimental progress in hydrogen pellet injection into tokamak discharge reveals a possibility of energy confinement improvement by intensive particle fueling at the plasma center. Namely, the pellet injection is not only a method of particle fueling but also the way of confinement improvement by altering the plasma density profile.

Pellet injection was found to improve the energy confinement time $\tau_E$ of high density Ohmic heating discharges of Alcator-C, where $\tau_E$ shows saturation against plasma density for gas puffing case. Alcator-C pellet fueling discharges demonstrated the $n_e \times \tau_E$ necessary for the break-even condition [1].

Improvement of energy confinement during neutral beam injection for limiter discharge was first demonstrated in Doublet-III, although the results showed mostly transient nature [2]. The application of pellet injection in large tokamak was initiated in TFTR. So far, the improvement of the global energy confinement time is very modest, although the confinement improvement at the plasma core is discussed for the discharges with energy confinement time satisfying slightly above the break-even condition, particularly when the plasma density has a strongly peaked profile with pellet fueling [3].

This paper discuss the pellet injection into JT-60 plasmas. The objectives of the present study are; 1) to evaluate the necessary pellet injector parameter for JT-60, 2) to evaluate the optimum operation scheme for the fueling near the plasma center, and 3) to study the modification of fusion power multiplication under particular assumption on energy and particle transport. The section 2 discuss the ablation profile for different plasma condiction, section 3

discuss the optimized operation scenario, section 4 investigates the pellet injection effects on fusion power multiplication using One-Dimensional tokamak code. The conclusion is given in section 5.

## 2. Description of Models

### 2.1 Pellet Ablation Model

A pellet injected into plasma ablates mainly by the bombardment of electrons. Numerous models describing the ablation rate of the pellet have already been proposed. Most valid models of them are neutral gas shielding one by Milora [4] and transonic neutral shielding one by Parks et al. [5]. In the present paper, we take Milora's model. In this model, the pellet is evaporated by the energetic plasma electrons incident to its surface, and the resultant neutral cloud surrounds the pellet. Thereafter, the incoming plasma electrons lose energy through inelastic collision with the neutral cloud, so that the pellet ablation is suppressed. In quasi-steady state that the residual electron energy flux on the pellet surface is balanced by the amount of cooling provided by the evaporated material, the pellet ablation rate $\frac{dd_p}{dt}$ is given in terms of the instantaneous pellet diameter $d_p(t)$, the plasma electron density $n_e$ and temperature $T_e$;

$$\frac{dd_p}{dt} = R(d_p, n_e, T_e) \tag{1}$$

During the travel after injection the pellet ablates in an inhomogeneous plasma of variable temperature and density. Owing to

discuss the optimized operation scenario, section 4 investigates the pellet injection effects on fusion power multiplication using One-Dimensional tokamak code. The conclusion is given in section 5.

## 2. Description of Models

### 2.1 Pellet Ablation Model

A pellet injected into plasma ablates mainly by the bombardment of electrons. Numerous models describing the ablation rate of the pellet have already been proposed. Most valid models of them are neutral gas shielding one by Milora [4] and transonic neutral shielding one by Parks et al. [5]. In the present paper, we take Milora's model. In this model, the pellet is evaporated by the energetic plasma electrons incident to its surface, and the resultant neutral cloud surrounds the pellet. Thereafter, the incoming plasma electrons lose energy through inelastic collision with the neutral cloud, so that the pellet ablation is suppressed. In quasi-steady state that the residual electron energy flux on the pellet surface is balanced by the amount of cooling provided by the evaporated material, the pellet ablation rate $\frac{dd_p}{dt}$ is given in terms of the instantaneous pellet diameter $d_p(t)$, the plasma electron density $n_e$ and temperature $T_e$;

$$\frac{dd_p}{dt} = R(d_p, n_e, T_e) \tag{1}$$

During the travel after injection the pellet ablates in an inhomogeneous plasma of variable temperature and density. Owing to

the cold electron added by the ablation, besides, the plasma temperature and density vary with time. To estimate the pellet penetration depth, these effects should be considered. The former is treated by dividing the plasma cross-section into toroidal shell of equal thickness in which the electron density and temperature can be regarded as being uniform. As an approximation of the latter, we adopt the self-limiting ablation model proposed by Houlberg et al. [6]. According to this model, the plasma temperature is adiabatically cooled by the addition of the ablatant. Since the pellet transit time in the shell is much longer than the electron-electron and ion-ion collision times, the pellet ablation rate is calculated by using the updated electron density and temperature every time step $\Delta t$ of the sufficiently small changes of the electron temperature and density. The total ablation in the shell $\Delta d_p$ is given by the sum of $R\Delta t$ over the pellet transit time in it $t_s=s/v_p$, where s and $v_p$ are the thickness of the shell and the pellet injection velocity, respectively. The pellet penetration depth is defined as a position where the pellet ablates completely. As seen from the previous discussion, the pellet penetration depth is determined by the pellet diameter, the pellet injection velocity, and the electron temperature and density distributions when the pellet is perpendicularly injected into the plasma towards the center.

The changes of the plasma density and temperature profiles after pellet injection are traced by using 1-D transport code. Since the time scales relevant to energy and particle transport are much greater than the time for total pellet ablation, the coupling of the pellet ablation code to 1-D transport code is made by delivering new plasma

density and temperature profiles calculated by the adiabatic approximation after a pellet injection.

## 2.2 1-D Transport Model

Tokamak transport code library, which is referred to as 'LIBRARY' [7], is the library system of the codes to analyze the transport process in the tokamak plasma and has the function of the interpretation on experimental data and the simulation of the thermo nuclear fusion plasma. In this simulation of the fusion power multiplication improvement with pellet injection, a 1-D transport code produced from 'LIBRARY' is able to calculate the hydrogenic-ion density profile, the electron and ion temperature profiles, the poloidal field profile, the neutral particle density profile, neutral beam injection, pellet injection and the sawtooth effect. The basic equations of the transport code are summarized as follows:

$$\frac{\partial n_i}{\partial t} = \frac{1}{r}\frac{\partial}{\partial r}(r\Gamma_i) - \frac{n_i}{\tau_{/\!/}} + S_i + S_{NB} \quad , \tag{2}$$

$$\frac{\partial}{\partial t}(\frac{3}{2} n_e T_e) = \frac{1}{r}\frac{\partial}{\partial r} r(n_e \chi_e \frac{\partial T_e}{\partial r} - \frac{3}{2} T_e \Gamma_e) - \gamma_e \frac{n_e T_e}{\tau_{/\!/}} - \frac{n_e(T_e - T_i)}{\tau_{eq}}$$

$$+ P_J + P_{NBe} - P_R \quad , \tag{3}$$

$$\frac{\partial}{\partial t}(\frac{3}{2} n_i T_i) = \frac{1}{r}\frac{\partial}{\partial r} r(n_i \chi_i \frac{\partial T_i}{\partial r} - \frac{3}{2} T_i \Gamma_i) - \gamma_i \frac{n_i T_i}{\tau_{/\!/}} + \frac{n_e(T_e - T_i)}{\tau_{eq}}$$

$$+ P_{NBi} - P_{CX} \quad , \tag{4}$$

$$\frac{\partial B_\theta}{\partial t} = \frac{\partial}{\partial t}\left(\frac{\eta}{\mu_o}\frac{1}{r}\frac{\partial}{\partial r}(rB_\theta)\right) . \qquad (5)$$

The equation (2) is the ion density continuity equation and $\Gamma_i$ is the particle flux in radial direction given as $\Gamma_i=-D_A\partial n_i/\partial r$, where $D_A$ is an anomalous diffusion coefficient and $n_i$ the ion density. $S_i$ and $S_{NB}$ are the source terms of cold neutrals and of fast neutrals due to the neutral beam injection, respectively. $\tau_{/\!/}$ is a loss time along to the magnetic field lines in the scrape-off region and given as $\pi qR_t/V_f$, where $R_t$ is the major radius, q the safety factor, and $V_f=\sqrt{T_e/m_i}$ an averaged flow velocity. Throughout this simulation, which does not treat impurities explicitly, the electron density is set $n_e=n_i$, although some appropriate fixed constant is chosen for the effective ionic charge $Z_{eff}$. The equations of (3) and (4) are the energy conservation equations for electrons and ions, respectively. $\chi_e$ is the electron thermal diffusivity and $\chi_i$ the ion one. $\tau_{eq}$ is the classical energy equipartition time between electrons and ions. The term $P_J$ denotes the joule input power given as $P_J=\eta_{/\!/}j^2$, where $\eta_{/\!/}$ is the classical resistivity with trapping corrections [8] and j the toroidal current. The terms $P_{NBe}$ and $P_{NBi}$ denote neutral beam heating of electrons and ions. The terms $P_R$ and $P_{CX}$ denote the power loss and gain related with neutral particles by ionization and charge exchange process for electrons and ions, respectively. The radiation loss due to the excitation is taken into account as the effective ionization loss with the ionization energy of 25 eV. The terms $\gamma_e$ and $\gamma_i$ denote the energy transmission coefficient across the sheath which is chosen to be 5.8 for electrons and 2.0 for ions. The equation (5) is the

poloidal field diffusion equation where $B_\theta$ is the poloidal field and $\mu_o$ the permeability of vacuum.

In order to simulate the sawtooth oscillations, the model given by Waddel et al. [9] is employed; island width W is presented as $W=W_0\exp[\int\gamma dt]$, where $W_0$ is the initial island width and $\gamma$ is the growth rate of the m/n=1/1 mode including the diamagnetic effect (m and n are poloidal and toroidal mode numbers, respectively). The magnetic flux exchange at the internal disruption follows the model proposed by Kadomtzev [10], while the profiles of temperatures and electron density are flattened under the conservation law.

The standard scalings for transport coefficients are used; as the electron thermal diffusivity, two kinds of scaling are employed, ie., $\chi_e=2\times10^{19}/n_e q$ for the joule heating plasma considered in section 3 and 4.1, and the improved INTOR scaling $\chi_e=2\times10^{19}/n_e$ for the neutral beam heating plasma studied in section 4.2 (this improved scaling is decided to allow the energy confinement time of 0.4 sec at the heating phase), $\chi_i$ for ions is from Hinton-Hazeltine [11] with a enhancement factor of five, particle diffusion coefficient $D_A=1\times10^{19}/n_e$ and particle recycling ratio R=0.9. $Z_{eff}$ is taken to be 1.5.

## 3. Parameter Surveys

We shall consider the perpendicular injection of a hydrogen pellet into a circular cross-section plasma. As described in the previous section, the variables which regulate the pellet penetration depth are the pellet diameter, the pellet injection velocity, and the electron temperature and density. In this section, we examine the dependence of the pellet penetration depth on these variables in order

poloidal field diffusion equation where $B_\theta$ is the poloidal field and $\mu_0$ the permeability of vacuum.

In order to simulate the sawtooth oscillations, the model given by Waddel et al. [9] is employed; island width W is presented as $W=W_0\exp[\int\gamma dt]$, where $W_0$ is the initial island width and $\gamma$ is the growth rate of the m/n=1/1 mode including the diamagnetic effect (m and n are poloidal and toroidal mode numbers, respectively). The magnetic flux exchange at the internal disruption follows the model proposed by Kadomtzev [10], while the profiles of temperatures and electron density are flattened under the conservation law.

The standard scalings for transport coefficients are used; as the electron thermal diffusivity, two kinds of scaling are employed, ie., $\chi_e=2\times10^{19}/n_e q$ for the joule heating plasma considered in section 3 and 4.1, and the improved INTOR scaling $\chi_e=2\times10^{19}/n_e$ for the neutral beam heating plasma studied in section 4.2 (this improved scaling is decided to allow the energy confinement time of 0.4 sec at the heating phase), $\chi_i$ for ions is from Hinton-Hazeltine [11] with a enhancement factor of five, particle diffusion coefficient $D_A=1\times10^{19}/n_e$ and particle recycling ratio R=0.9. $Z_{eff}$ is taken to be 1.5.

## 3. Parameter Surveys

We shall consider the perpendicular injection of a hydrogen pellet into a circular cross-section plasma. As described in the previous section, the variables which regulate the pellet penetration depth are the pellet diameter, the pellet injection velocity, and the electron temperature and density. In this section, we examine the dependence of the pellet penetration depth on these variables in order

to provide the pellet injection scenario forming the target plasma with highly peaked density for auxiliary heating. Numerical simulations are performed for the plasma parameters typical to JT-60 ohmically heated divertor discharges of 2 MA. The standard values used to the simulation are given in Table 1. The electron temperature profile was taken from Thomson scattering measurements, and the electron density profile was converted from the line integrated electron densities measured by a 2 mm microwave and 3 channel submillimeter interferometers. In the following calculations, the central electron temperature is fixed to the experimental value of 2 keV in order to facilitate the understanding of the pellet penetration. The electron density profile changes after the pellet injection since the pellet fueling produces the peaked electron density profile. The effect of the different electron density profile on the pellet penetration depth is discussed in a later section.

### 3.1 Requirements for Pellet Injection

The most important role of pellet fueling is to produce the centrally peaked electron density profile. The electron density profile changes strikingly depending on the pellet penetration depth. Figure 1 shows the effect of the pellet penetration depth on the electron density deposition profile when a hydrogen pellet of diameter 2.7 mm was injected into the standard plasma of the central electron density $3\times10^{19}/m^3$ listed in Table 1. The pellet penetration depth was controlled by varying the pellet injection velocity. It is seen from the figure that the highly peaked deposition profile can be obtained when the pellet passes through the plasma center. On the other hand, the complete penetration of the plasma almost always results in

disruption according to the pellet fueling experiment by Milora et al. [12]. To obtain the highly peaked electron density profile, therefore, the pellet penetration depth must be in the range of the plasma center to the opposite plasma edge for the perpendicular injection of a pellet into the plasma towards the center.

The use of a large pellet is of great advantage to penetrate deep into the plasma with lower injection velocity, while it causes strong perturbations in the electron density and temperature. The upper limit of the pellet size on the stable fueling is not clear. According to the pellet injection experiment in TFTR, however, it is possible to fuel stably up to the pellet which contains the hydrogen atoms equal to the total number of electrons in the plasma before injection. Here, we choose the equivalent of the whole electrons in the plasma as the maximum pellet size capable of injecting.

The last restriction for the pellet injection is of technical requirement. Two types of pellet injectors have practical application. One is a gun-type pneumatic injector, and the other is a centrifuge injector. The high speed injection is essential especially for large tokamak to achieve the deep penetration into the plasma. On this viewpoint, a gun-type pneumatic pellet injector with a maximum velocity 1.9 Km/s is suitable. Since the maximum pellet velocity corresponds to about 80% of the theoretical limit derived from the ideal gun theory proposed by Milora et al. [13], the upper limit of the pellet injection velocity available is assumed to be 2km/s, which is a modest extrapolation from the present technical level.

3.2 Optimum Conditions of Pellet Injection

In the present study, the variables which determine the pellet penetration depth are three of the pellet diameter, the pellet injection velocity and the electron density because of a fixed electron temperature. When the pellet diameter among them is given, an area which satisfies three requirements for the pellet injection in an orthogonal coordinate system with the electron density and the pellet injection velocity as the coordinate axes is defined as a pellet operation area. Figure 2 shows the pellet operation areas (the shadowed portions) for four pellet diameters of 2.7, 3.0, 3.5 and 4.0 mm. In the figure, the upper curve with a sign $a_p$ presents the relation between the averaged electron density and the pellet injection velocity required to inject the pellet up to the plasma center, and the lower one marked by $2a_p$ is that required for the pellet to reach the opposite plasma edge across the center. The dotted line indicates the electron density equivalent to the whole sum of electrons included in a solid hydrogen pellet.

The pellet operation area spreads rapidly in spite of the increase of the lower limit of the electron density capable of injecting as the pellet diameter increases. From this figure, it is obvious that the target plasma with the averaged electron density of $6\times10^{19}/m^3$ can be formed from the initial ohmic plasma with that of $2\times10^{19}/m^3$ by combining a few pellet with the different radius. Further extension of the pellet operation area could be achieved by developing the pellet injector with the injection velocity above 2 km/s.

Since the electron density profile changes after pellet injection, the effect of the variation in the profile on the pellet

operation area was examined. Figure 3 shows the pellet operation areas for the flat electron density typical of the ohmically heated divertor plasma in JT-60 and the peaked density profile given by $n_e(r)/n_{eo}=0.9[1-(\frac{r}{a_p})^2]^2+0.1$ for two pellet diameters of 2.7 and 4.0 mm. The shift of the latter pellet operation area to right-hand side is at best 5%, which could be sufficiently neglected for the production of pellet injection scenario.

Figure 4 shows the pellet operation areas at three central electron temperatures of 1, 2 and 3 keV for two pellet diameters of 2.7 and 4.0 mm. The pellet operation area varies remarkably depending on the electron temperature. Since the electron temperature changes greatly after pellet injection, special attention should be paid to timing of next pellet injection.

### 3.3 Time Evolution of Density and Temperature after Pellet Injection

The recovery time of the electron temperature is a important quantity to judge the timing of next pellet injection because the pellet injection before that corresponds to the large pellet injection which may result in disruption as mentioned in Sec. 3.1. Therefore, the time evolution of the electron density and temperature after pellet injection was traced by using 1-D transport code. An example in which a pellet of diameter 3.5 mm with the velocity of 1.2 km/s is injected into the plasma of the central electron temperature 2 keV and density $2.5\times10^{19}/m^3$ is shown in Fig. 5. In the figure, the ordinates are volume averaged electron density and density averaged electron temperature. The electron temperature recovers to the previous level

in 320 ms after pellet injection. Then, pellet fueled electron density decreases by approximately 60 %, which is almost independent of the pellet size and the electron density before pellet injection. The recovery time of the electron temperature versus the pellet diameter is shown in Fig. 6. As expected, the recovery time of the electron temperature increases with the pellet diameter, but it scarcely depends on the previous level of the electron density. As a result, the decay rate of the additional density and the recovery time of the temperature are not affected by the electron density before pellet injection and moreover, the former is independent of the pellet size. These facts are useful to provide the scenario for the multi-pellet injection.

Figure 7 shows the deformation of the peaked electron density profile with time after pellet injection for two pellet diameters of 2.7 and 4.0 mm. It is seen from the figure that the larger pellet leads to longer hold of the peaked density profile. This means that the large pellet ablates mainly in the central portion of plasma comparing with the small one. Therefore, it is desirable to use the pellet as large as possible in the permitted limit.

## 4. Numerical Results

A serial pellet injection during auxiliary heating is desirable to maintain the peaking profile of electron density. However, the auxiliary heated plasma with high temperature will not allow a pellet to penetrate to the plasma center. Hence, we consider to produce the peaked density profile beforehand.

in 320 ms after pellet injection. Then, pellet fueled electron density decreases by approximately 60 %, which is almost independent of the pellet size and the electron density before pellet injection. The recovery time of the electron temperature versus the pellet diameter is shown in Fig. 6. As expected, the recovery time of the electron temperature increases with the pellet diameter, but it scarcely depends on the previous level of the electron density. As a result, the decay rate of the additional density and the recovery time of the temperature are not affected by the electron density before pellet injection and moreover, the former is independent of the pellet size. These facts are useful to provide the scenario for the multi-pellet injection.

Figure 7 shows the deformation of the peaked electron density profile with time after pellet injection for two pellet diameters of 2.7 and 4.0 mm. It is seen from the figure that the larger pellet leads to longer hold of the peaked density profile. This means that the large pellet ablates mainly in the central portion of plasma comparing with the small one. Therefore, it is desirable to use the pellet as large as possible in the permitted limit.

## 4. Numerical Results

A serial pellet injection during auxiliary heating is desirable to maintain the peaking profile of electron density. However, the auxiliary heated plasma with high temperature will not allow a pellet to penetrate to the plasma center. Hence, we consider to produce the peaked density profile beforehand.

4.1 Production of Target Plasma for Auxiliary Heating

If a pellet injection is made immediately after the recovery of electron temperature, the production scenario of the target plasma with the electron density exceeding $6\times10^{19}/m^3$ can be determined from the optimum condition of pellet injection and the recovery time of the electron temperature. We shall consider three cases of the pellet injection scenario. In the case I, the pellet injector can fire several kinds of pellet with the different diameter at arbitrary velocity below 2 km/s. In the case II, only the pellet injection velocity is fixed. Case III treats a scenario for the injector with fixed pellet diameter and injection velocity. Four pellet diameters of 2.7, 3.0, 3.5 and 4.0 mm are chosen as a typical size. The pellet size of the first injection into the gas fueled plasma is chosen among them by referring the pellet operation area. If it is possible to inject the pellet of unequal size more than two, the largest pellet is taken in order to extend the hold period of the peaked density profile. The average value in the permitted range is selected as a pellet injection velocity, but in the case II, III, the maximum of the pellet injection velocity available is used to enable to inject the pellet of the same size to the plasma with higher density in next step. Next pellet injection is made after the recovery of the electron temperature, and then, the electron density is given by the sum of the previous one and 60% of the amount increased by the pellet. The pellet size of second injection is selected for a new electron density. This process is repeated until the electron density immediately after injection satisfys the plasma density level required for the auxiliary heating. The pellet injection scenarios of three cases determined thus are summarized in Table 2. In the case III with

the restrictions of the fixed pellet size and injection velocity, the initial density becomes inevitably higher due to the narrow pellet operation area for a single pellet size.

The time evolution of the volume averaged electron density and the electron density profile after the final pellet injection were calculated by using 1-D transport code and pellet ablation code when the pellet is injected according to the scenario described above. The simulation results of cases I, II and III are shown in Figs. 8, 9 and 10, respectively. In three cases, the volume averaged electron density above $6\times10^{19}/m^3$ is obtained by the final pellet injection, and thereafter, the peaked electron density profile is maintained over 0.5 s. As expected, each of pellets injected reaches the range between the plasma center and the opposite plasma edge. These results indicate that the pellet injection scenario is effective to attain the directing high density with the peaked profile by the pellet fueling.

## 4.2 1-D Tokamak Simulation of Fusion Power Multiplication Factor Improvement with Pellet Injection

Result of equivalence break even scenario calculation by pellet injection are presented that were obtained in the frame work of an assessment performed for JT-60, and are compared with results corresponding to gas puffing.

The fusion power multiplication in a hydrogen plasma is calculated as an equivalence fusion plasma with the same fraction rate of densities of deutrium and tritium, without the beam-plasma reaction (TCT effect). Then the fusion power multiplication factor Q is defined as $Q=\int n_i^2/4\langle\sigma v\rangle Q_T dV/P_{in}$, in which $\langle\sigma v\rangle$ is the D-T fusion

reaction rate and $Q_T$ the reaction energy of 17.6 MeV and $P_{in}$ the total input power. The fusion power is not reflected to the calculation of plasma temperatures. The beam energy of 100 keV ($H^0$ particles) and the beam power of 20 MW are considered.

Figure 11 shows the time evolution of the volume average electron density fueled by the pellet injection, according to the case-I in table 2, in which three pellets are injected, successively, at 0.9 sec, 1.13 sec and 1.45 sec, and the neutral beam heating starts at 1.5 sec. The volume density reaches to about $7.0\times10^{19}$ $m^{-3}$ at 1.45 sec and is on the decrease in the neutral beam heating phase, because of the particle recycling ratio of 0.9. The case of gas puffing with the particle flux of $2\times10^{21}$ $s^{-1}$ is also shown as dotted line in Fig. 11. Both volume densities become same about $5.2\times10^{19}$ $m^{-3}$ at about 2.8 sec, and then the fusion power multiplication factor by pellet injection is in excess of about 0.2 comparing with the one by gas puffing as shown in Fig. 12-a. Figures 12-b, -c and -d show the profiles of the electron density, the ion temperature and the heat deposition of ions at t=2.8 sec. The peaked density profile has the advantage to have deep NB penetration and maintain favourable heat deposition profile. The improved neutral beam penetration is responsible for the almost same ion temperature around the plasma center as shown in Fig. 12-c and produces the higher Q value at the same volume average density. Figure 13 shows the evolution of temperatures and the density at the center. After starting the neutral beam heating, the drop of temperatures and the density due to the sawtooth oscillation are seen and the Q value decreases slightly at that time. In this calculation, the temperatures and the density recover in about 0.6 sec after the occurrence of the sawtooth and the Q value keeps almost constant

during the recovering phase. Therefore, it can be considered that there is little effect of the sawtooth oscillation on the thermo nuclear fusion reaction.

When the density keeps increasing due to the gas puffing, the high Q value which is comparable to the one by the pellet injection is obtained at the high density of $7\times10^{19}$ $m^{-3}$, as shown in Fig. 11-a. The energy confinement time is, however, about 0.55 sec in such a high density. From many results of the neutral beam heating experiments [14,15], it is too optimistic to rely on such a good confinement time for attaining the break even condition. Therefore, it is important that a high Q value is obtained in a relatively lower density and energy confinement time by the pellet injections. According to the 0-dimensional analysis by NIIKURA [16], the contribution of the beam-plasma reaction to the Q will be expected to be about 0.5 with 100 KeV deuterium beam. Including the TCT effect, the pellet injection will be a great help in reaching the equivalence break even of Q~1.

## 5. Conclusions

Ablation of hydrogen ice pellet in the JT-60 plasma was calculated by ORNL pellet ablation code, which employs a neutral gas shielding model. An optimum operation scheme to produce central peaked $n_e$ profile of $n_e(0) = 2\times10^{20}$ $m^{-3}$ and $n_e(0)/\langle n_e\rangle \sim 3$ in the ohmic discharge appears to be a pellet injection with the pellet size of 3.4 mm diameter and velocity of 2 km/s.

Under the assumption of electron heat diffusivity $\chi_a=2\times10^{19}/n_e q$ ($m^2/s$), the 1D tokamak code (LIBRARY) predicts ~30 % increment of fusion multiplication (Q) for pellet fueled peaked density profile

during the recovering phase. Therefore, it can be considered that there is little effect of the sawtooth oscillation on the thermo nuclear fusion reaction.

When the density keeps increasing due to the gas puffing, the high Q value which is comparable to the one by the pellet injection is obtained at the high density of $7\times10^{19}$ $m^{-3}$, as shown in Fig. 11-a. The energy confinement time is, however, about 0.55 sec in such a high density. From many results of the neutral beam heating experiments [14,15], it is too optimistic to rely on such a good confinement time for attaining the break even condition. Therefore, it is important that a high Q value is obtained in a relatively lower density and energy confinement time by the pellet injections. According to the 0-dimensional analysis by NIIKURA [16], the contribution of the beam-plasma reaction to the Q will be expected to be about 0.5 with 100 KeV deuterium beam. Including the TCT effect, the pellet injection will be a great help in reaching the equivalence break even of Q~1.

## 5. Conclusions

Ablation of hydrogen ice pellet in the JT-60 plasma was calculated by ORNL pellet ablation code, which employs a neutral gas shielding model. An optimum operation scheme to produce central peaked $n_e$ profile of $n_e(0) = 2\times10^{20}$ $m^{-3}$ and $n_e(0)/\langle n_e\rangle \sim 3$ in the ohmic discharge appears to be a pellet injection with the pellet size of 3.4 mm diameter and velocity of 2 km/s.

Under the assumption of electron heat diffusivity $\chi_a=2\times10^{19}/n_e q$ ($m^2/s$), the 1D tokamak code (LIBRARY) predicts ~30 % increment of fusion multiplication (Q) for pellet fueled peaked density profile

compared with gas fueled discharge. In the pellet fueling experiment in JT-60, which is now planed in 1988, more enhancement of Q than the code prediction will be anticipated due to the experimentally observed favorable energy confinement for peaked density profile discharge.

Acknowledgements

We wish to express our appreciation to Drs. Y. Shimomura and M. Azumi for fruitful discussions. The continuing support of Drs. S. Mori, K. Tomabechi, M. Yoshikawa and T. Iijima, is geatefully acknowledged.

compared with gas fueled discharge. In the pellet fueling experiment in JT-60, which is now planed in 1988, more enhancement of Q than the code prediction will be anticipated due to the experimentally observed favorable energy confinement for peaked density profile discharge.

Acknowledgements

We wish to express our appreciation to Drs. Y. Shimomura and M. Azumi for fruitful discussions. The continuing support of Drs. S. Mori, K. Tomabechi, M. Yoshikawa and T. Iijima, is geatefully acknowledged.

References

1) M. Greenwald, D. GWinn, S. Milora, J. Parker, R. Parker, et al., in Plasma Physics and Controlled Nuclear Fusion Research 1984 (Proc. 10th Int. Conf. London, 1984), Vol.1, IAEA, Vienna (1985) 45.

2) S. Sengoku, M. Nagami, M. Abe, K. Hoshino, A. Kameari, et al., Nucl. Fusion 10 (1985) 1475.

3) S.J. Zweben, M.H. Redi, G. Bateman, Princeton University Plasma Physics Laboratory Report PPPL-2316 (1986).

4) S.L. Milora, ORNL/TM-8616 (1983).
S.L. Milora and C.A. Foster, ORNL/TM-5776 (1977).

5) P.B. Parks and R.J. Turnbull, Phys. Fluids 21 (1978) 1735.

6) W.A. Houlberg, M.A. Iskra, H.C. Home and S.E. Attenberg, ORNL/TM7 6549 (1979).

7) T. Hirayama, et al. Library system for a one dimensional tokamak transport code (LIBJT60), JAERI-M 82-204, (1982).

8) S.P. Hirshman, R.J. Hawryluk, B. Birge, Neoclassical conductivity of a Tokamak Plasma, PPPL-1326, (1977).

9) B.V. Waddel, G.L. Jhans, J.D. Callen, et al., ORNL/TM-5840 (1977).

10) B.B. Kadomtzev, Sov. J. Plasma Phys., 1, (1975) 389.

11) T.L. Hinton, R.D. Hazeltine, Rev. Mod. Phys. 48 (1976) 239.

12) S.L. Milora, C.A. Foster, et al., Nucl. Fusion 20 (1980) 1491.

13) S.L. Milora and C.A. Foster, Rev. Sci. Instrum. 50 (1979) 482.

14) F. Wagner, et al., 12th Europe. Conf. on Cont. Fus. and Plasma, (Budapest, 1985), Vol. I, 335.

15) M. Murakami, et al., PPPL-2224.

16) S. Niikura, M. Nagami, T. Hirayama, JAERI-M 86-089, (1986).

Table 1 Standard values used to numerical simulation

| Parameters | Standard values |
|---|---|
| Plasma major radius, $R_p$ | 3.15 m |
| Plasma minor radius, $a_p$ | 0.87 m |
| Plasma current, $I_p$ | 2 MA |
| Central Electron temperature, $T_{eo}$ | 2.0 keV |
| Temperature profile, $T_e(r)/T_{eo}$ | $0.95\left[1-\left(\frac{r}{a_p}\right)^2\right]^{1.5}+0.05$ |
| Density profile, $n_e(r)/n_{eo}$ | $0.9\left[1-\left(\frac{r}{a_p}\right)^2\right]^{0.3}+0.1$ |
| Plasma species | Hydrogen |
| Pellet species | Hydrogen |

Table 2 Pellet injection scenarios to produce the target plasma for auxiliary heating

| Cases | Items: Injections | Injection time (s) | Electron density ($10^{19}/m^3$) | Pellet diameter (mm) | Injection velocity (km/s) |
|---|---|---|---|---|---|
| Case I | 1st | 0 | 2.0 | 3.0 | 1.8 |
| | 2nd | 0.23 | 3.0 | 3.5 | 1.6 |
| | 3rd | 0.55 | 4.6 | 3.5 | 2.0 |
| Case II | 1st | 0 | 2.0 | 3.0 | 1.9 |
| | 2nd | 0.23 | 3.0 | 3.5 | 1.9 |
| | 3rd | 0.55 | 4.6 | 3.5 | 1.9 |
| Case III | 1st | 0 | 3.0 | 3.5 | 1.8 |
| | 2nd | 0.32 | 4.6 | 3.5 | 1.8 |

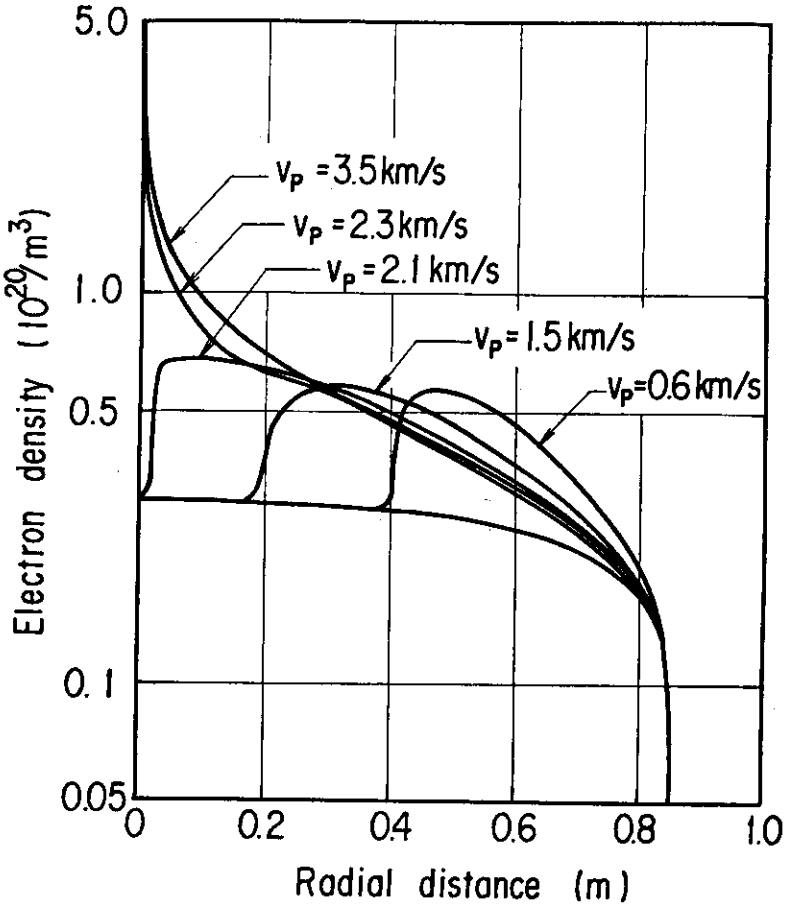


Fig. 1 The relation between the electron density deposition profile and the pellet penetration depth.

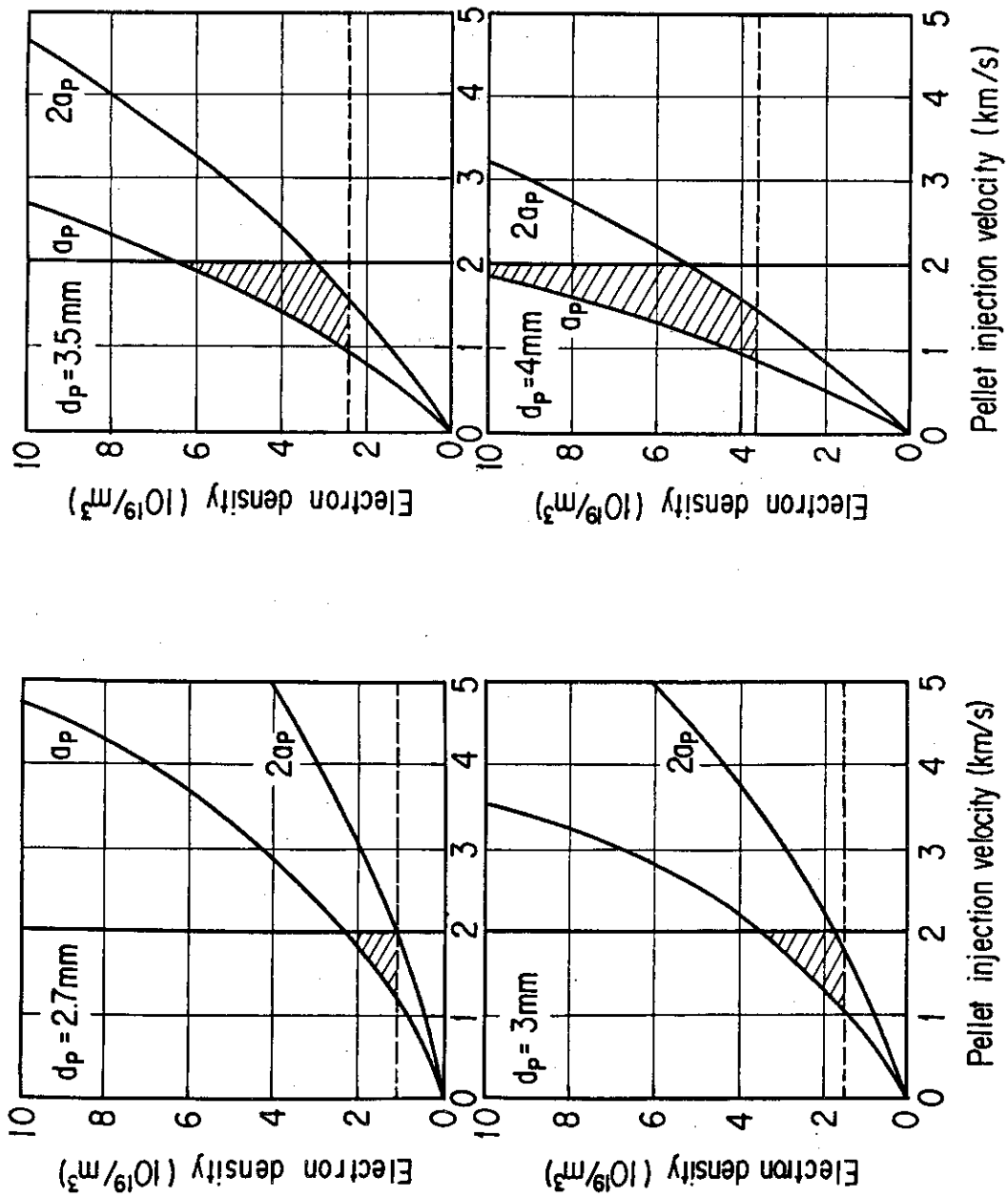


Fig. 2 The pellet operation areas for four pellet diameters of 2.7, 3.0, 3.5 and 4.0 mm

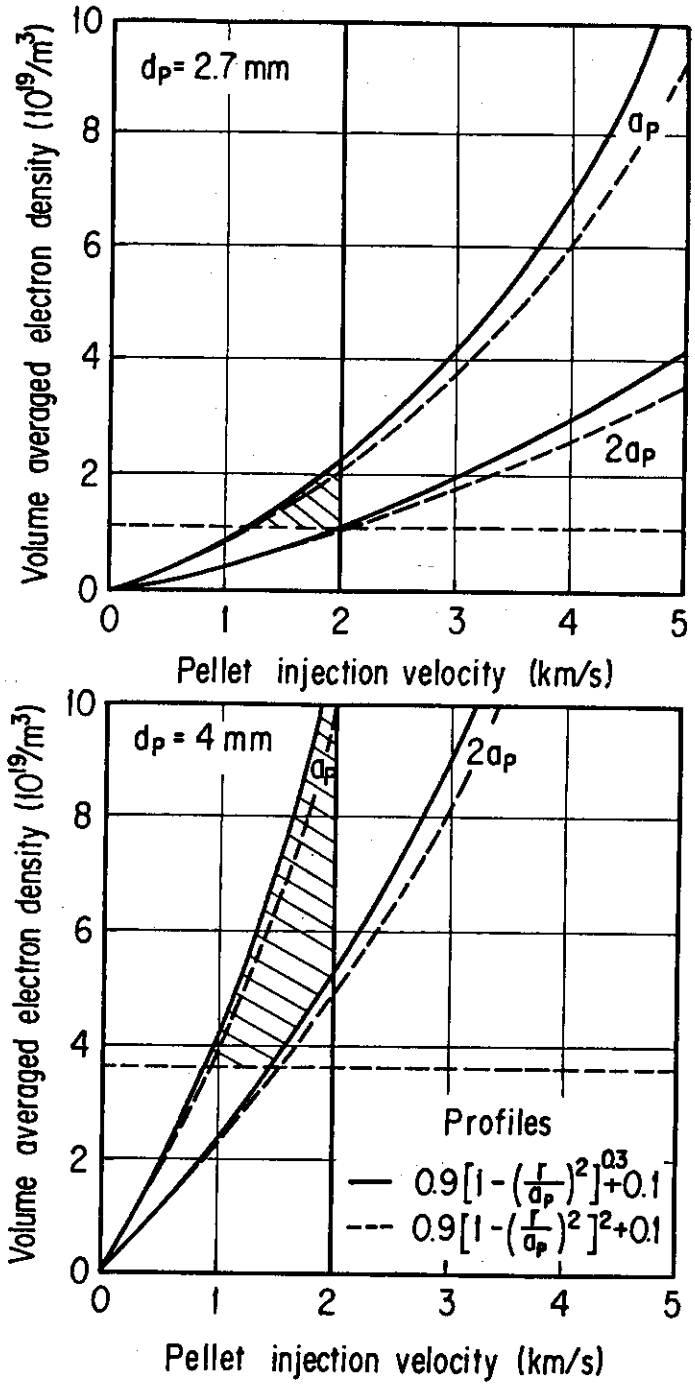


Fig. 3 The effect of the difference in electron density profile on the pellet operation area.

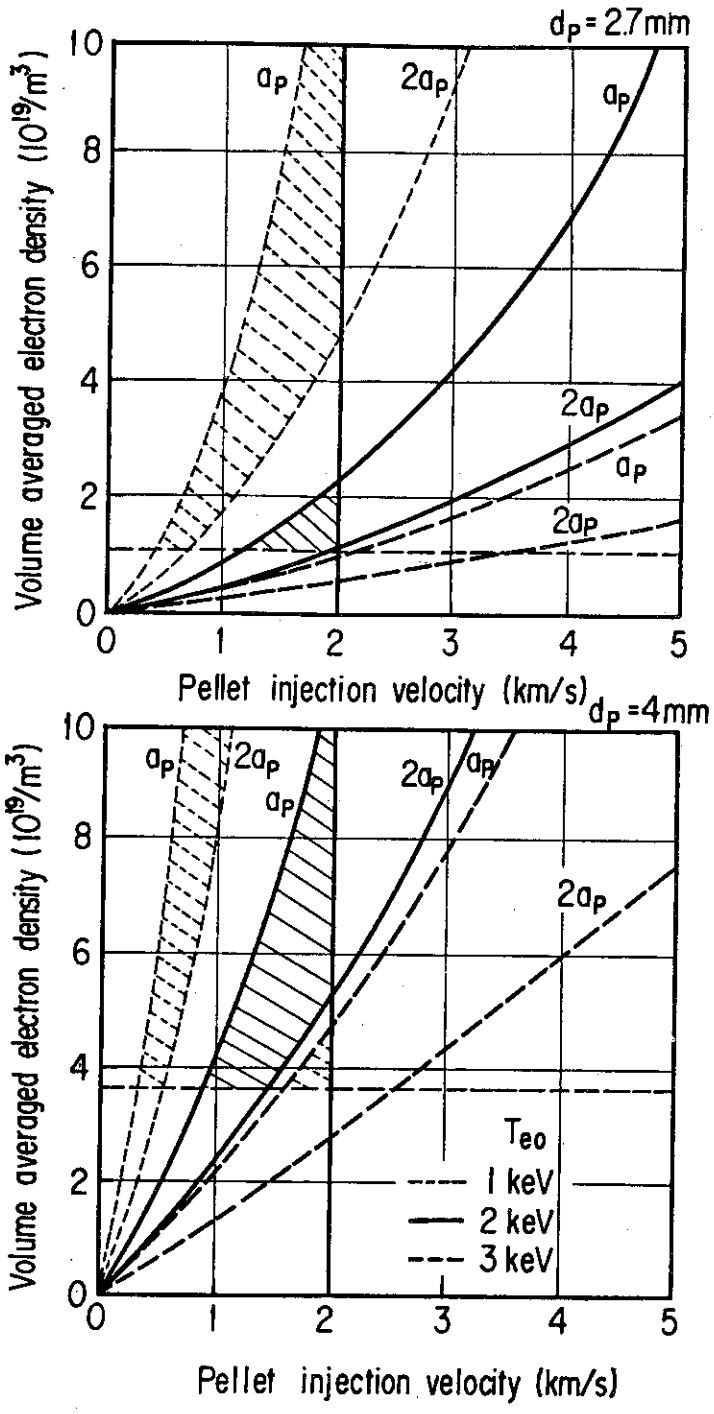


Fig. 4 The variation of the pellet operation area against the central electron temperature.

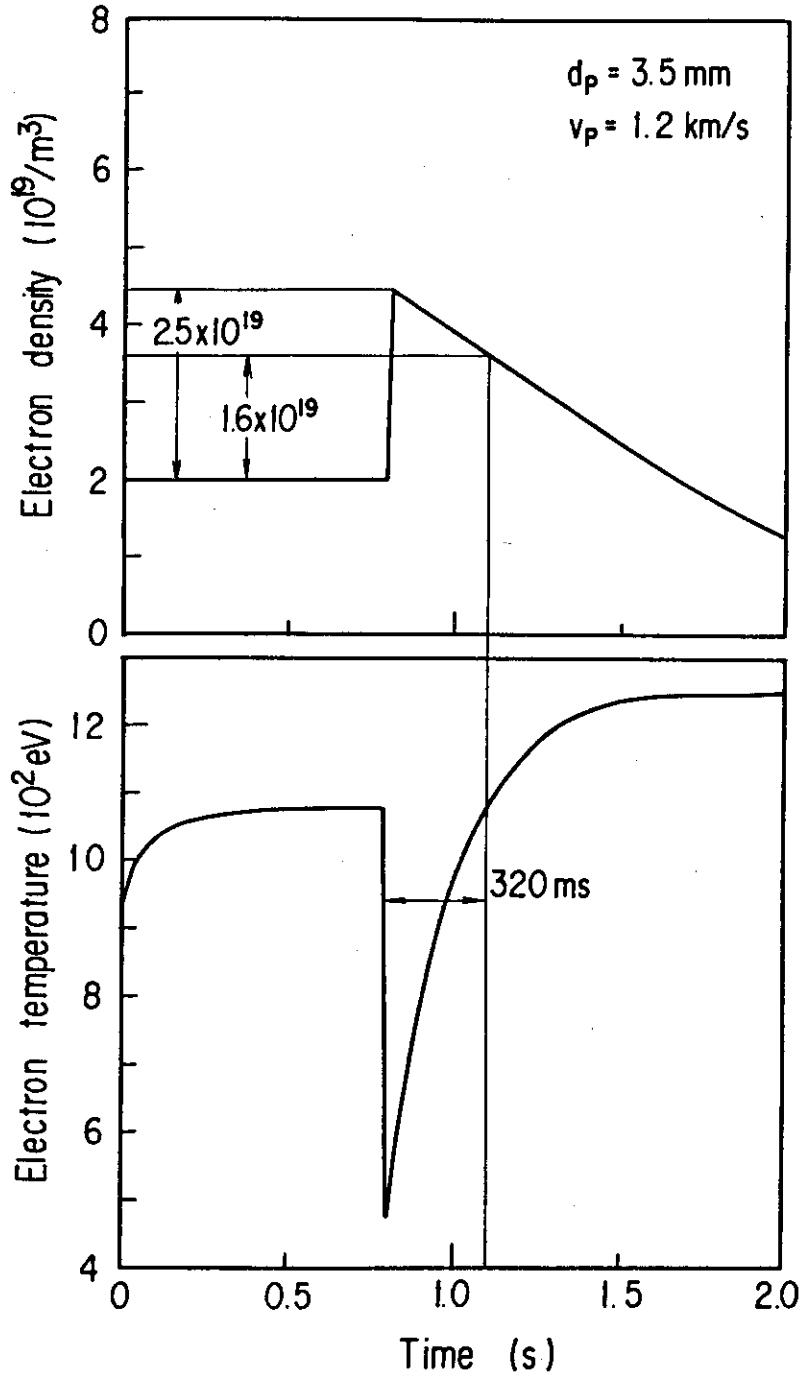


Fig. 5 An example of the time evolution of density and temperature after a pellet injection.

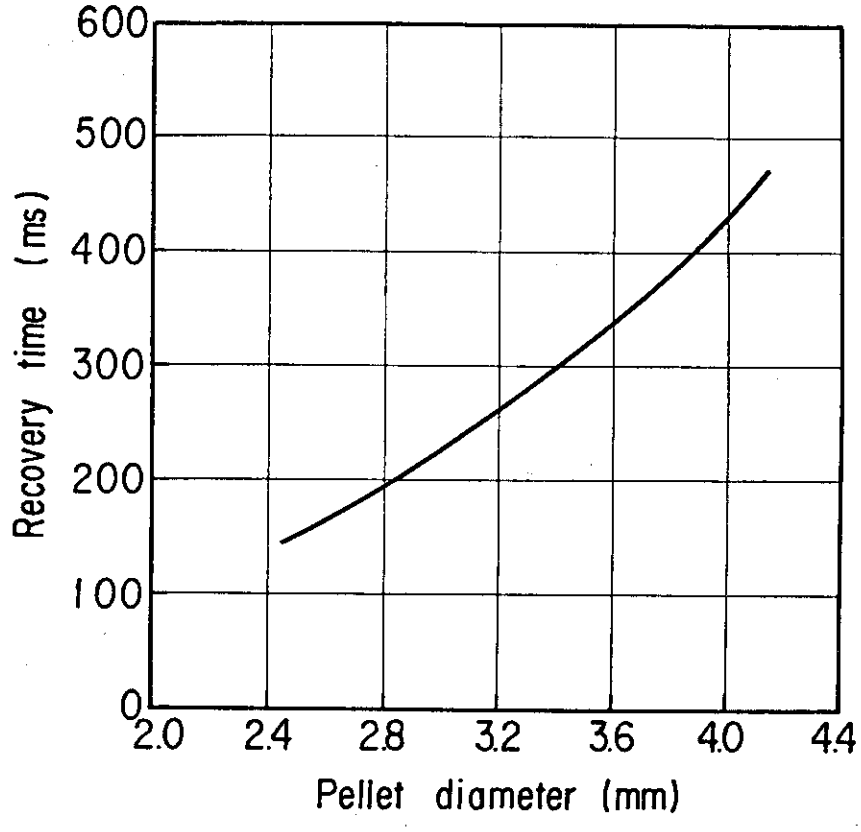


Fig. 6 The recovery time of the electron temperature after injection versus pellet diameter.

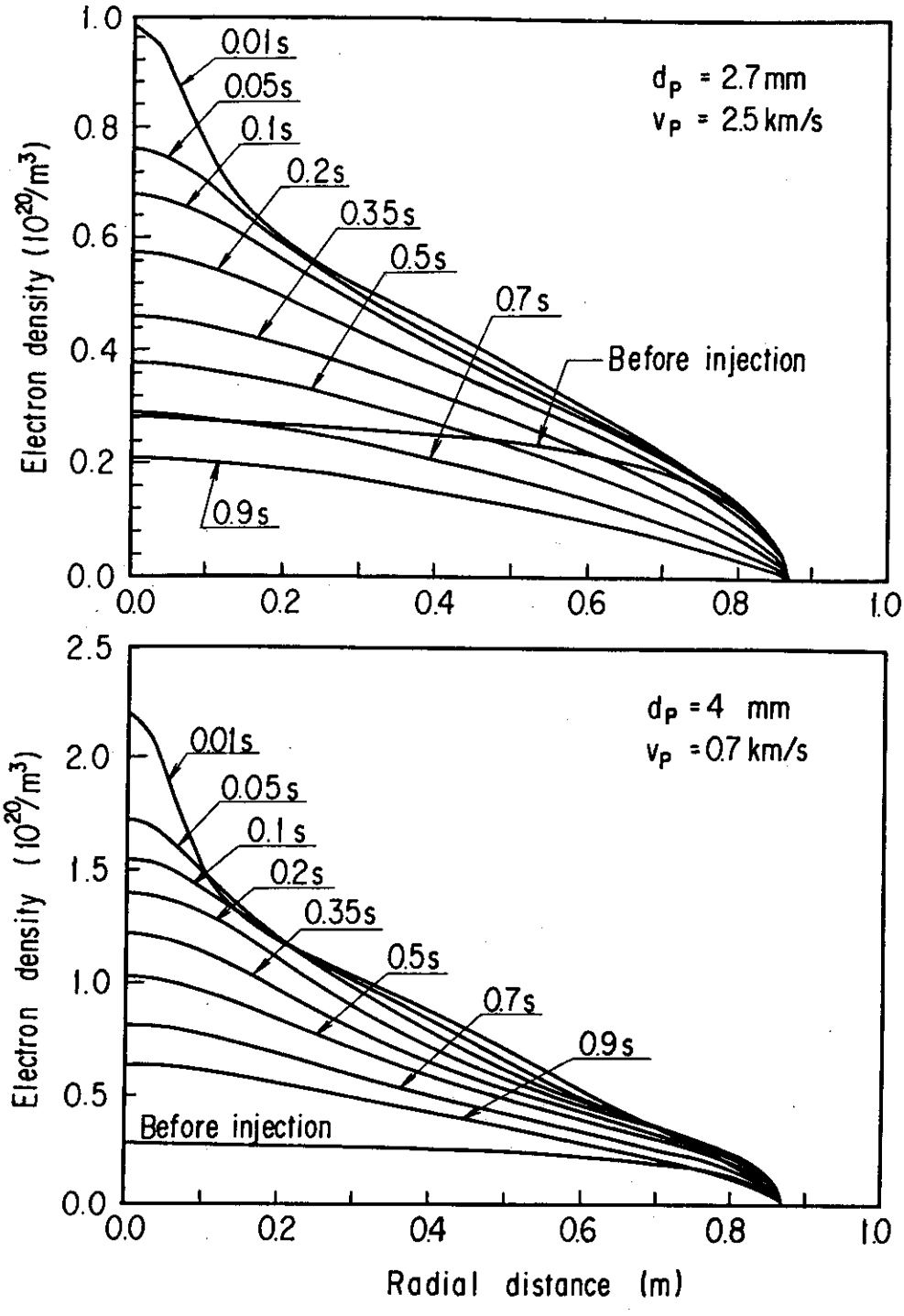


Fig. 7 The deformation of the peaked electron density profile after a pellet injection with time.

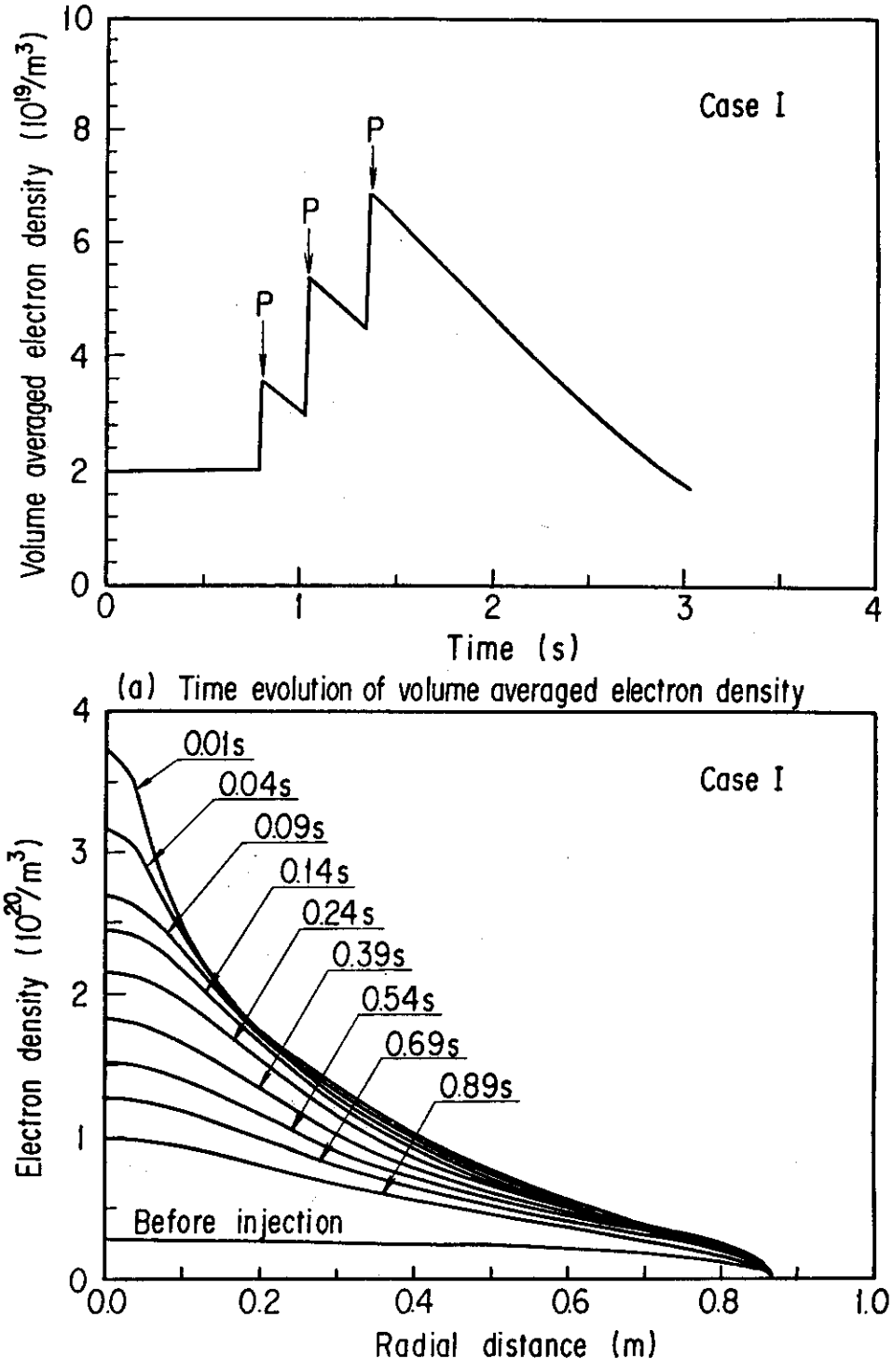


Fig. 8 The simulation results for the case I of the pellet injection scenario.

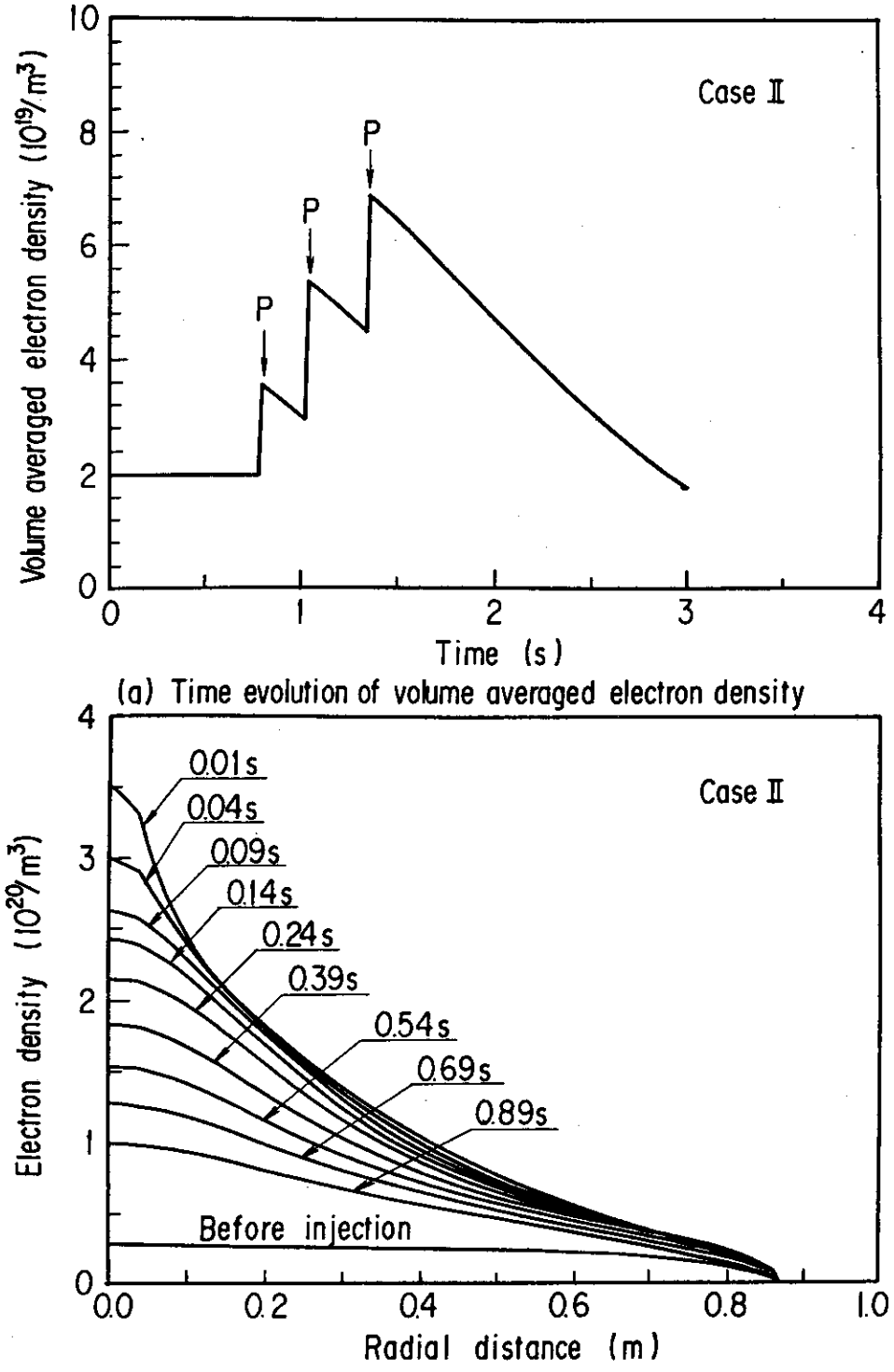


Fig. 9 The simulation results for the case II of the pellet injection scenario.

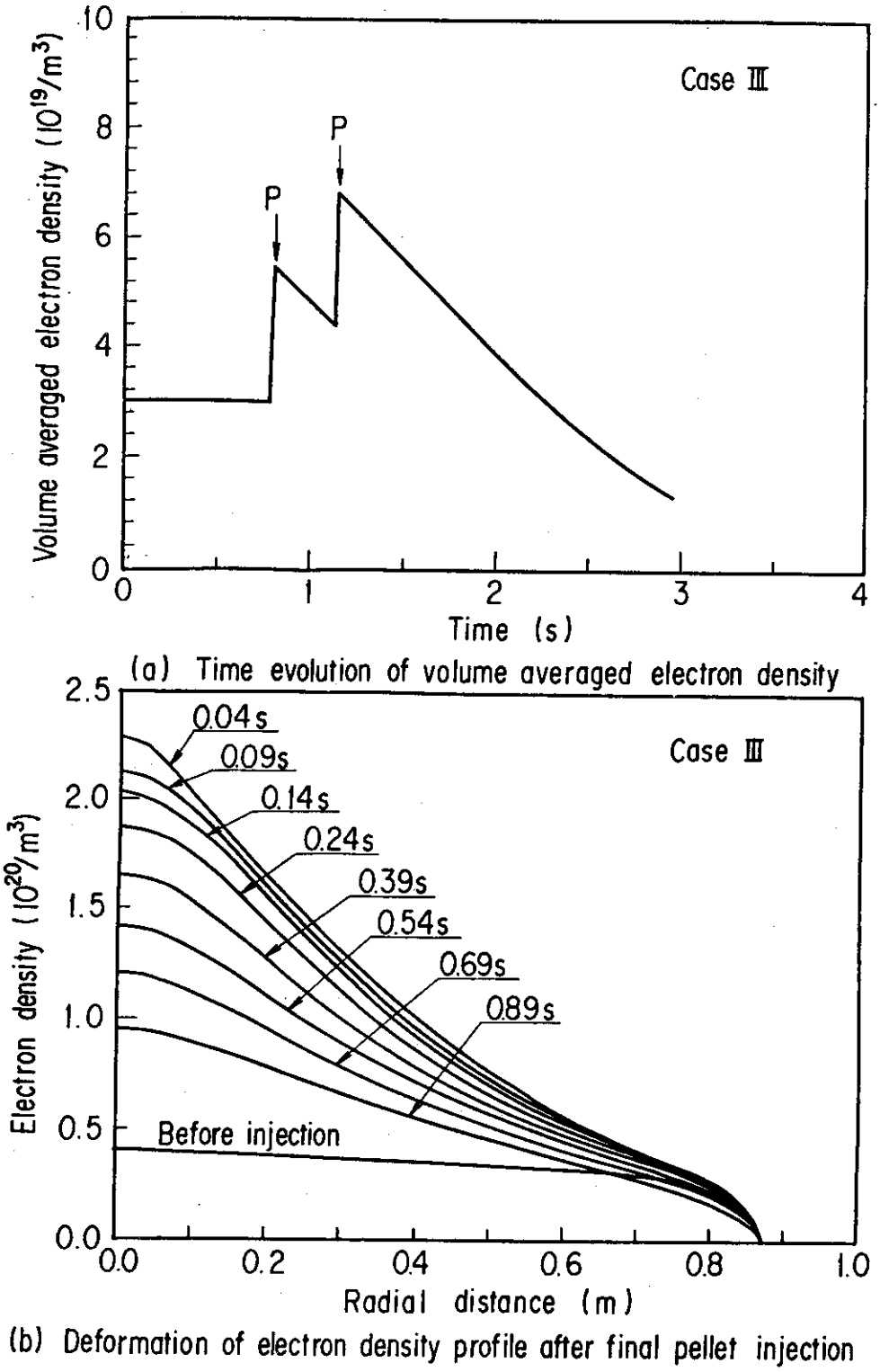


Fig.10 The simulation results for the case III of the pellet injection scenario.

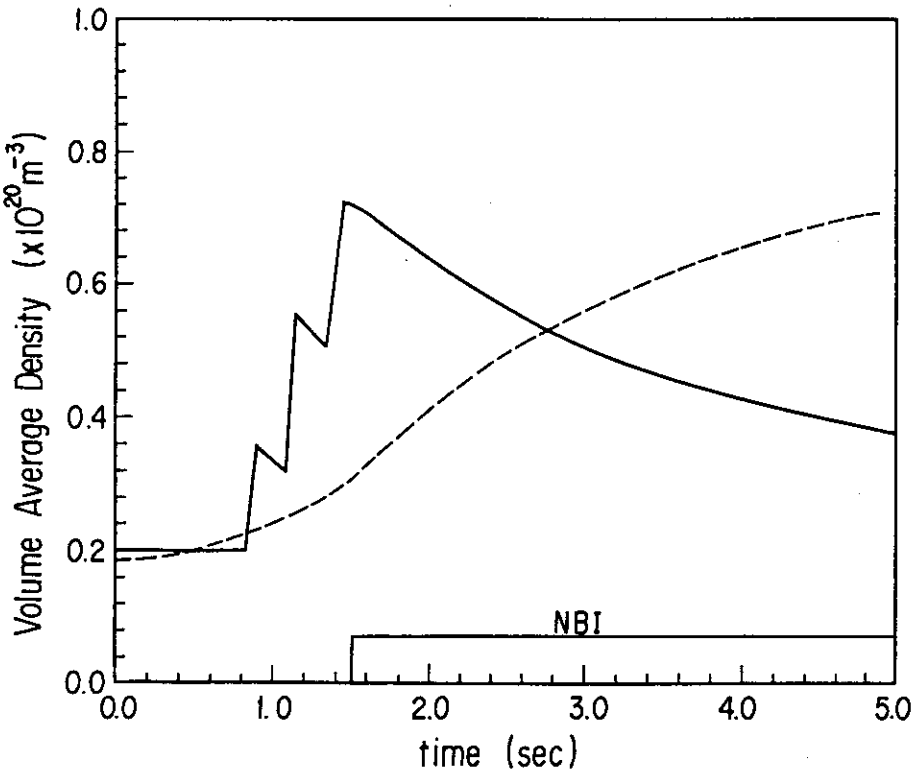


Fig.11 Time evolution of the volume averaged density. The solid line shows the case of pellet injection, in which three pellets are injected, successively, at 0.9 sec, 1.13 sec and 1.45 sec, according to the Case-I. The dotted line shows the case of gas puffing with the particle flux of $2\times10^{21}$ $s^{-1}$.

Fig. 12-a

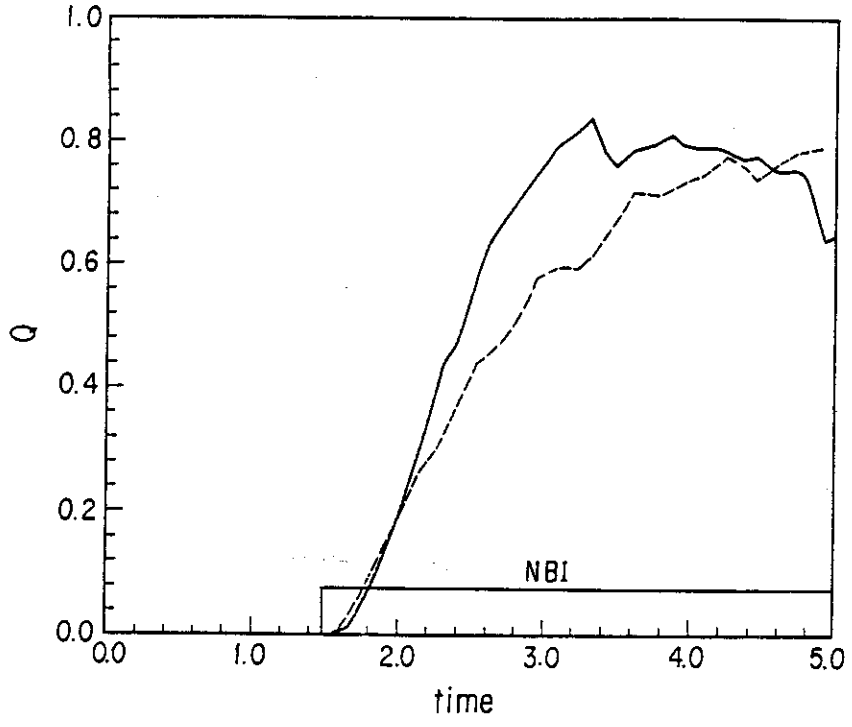


Fig. 12-b

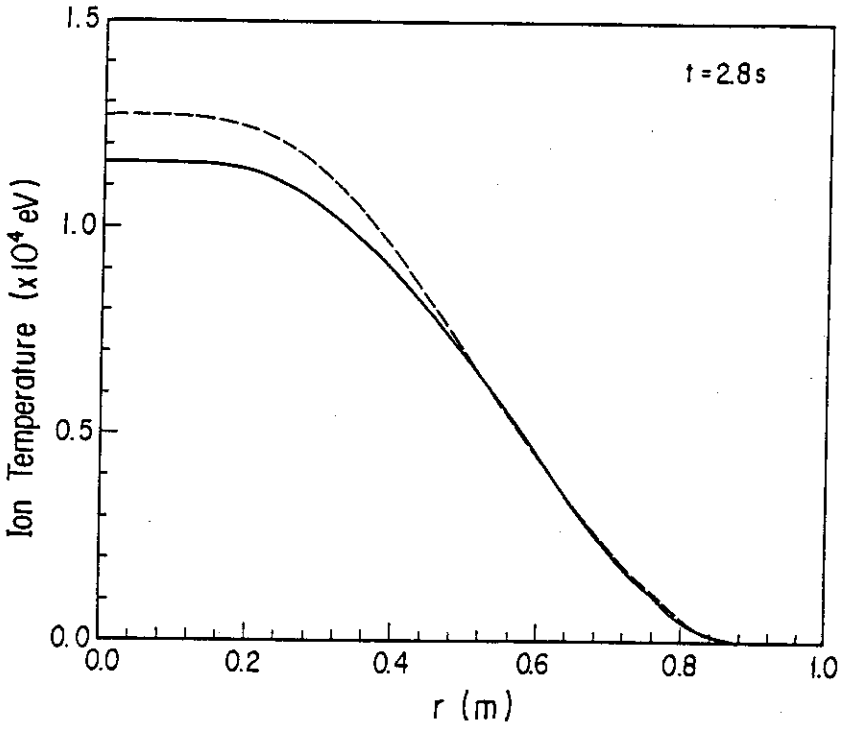


Fig.12 The solid line shows the case of pellet injection and the dotted line shows the case of gas puffing with the particle flux of $2\times10^{21}$ $s^{-1}$: a); the time evolution of the fusion power multiplication factor Q, b); the electron density profile obtained at 1.3 sec after the neutral beam injection, c); the ion temperature profiles, d); the heat deposition profiles of ion.

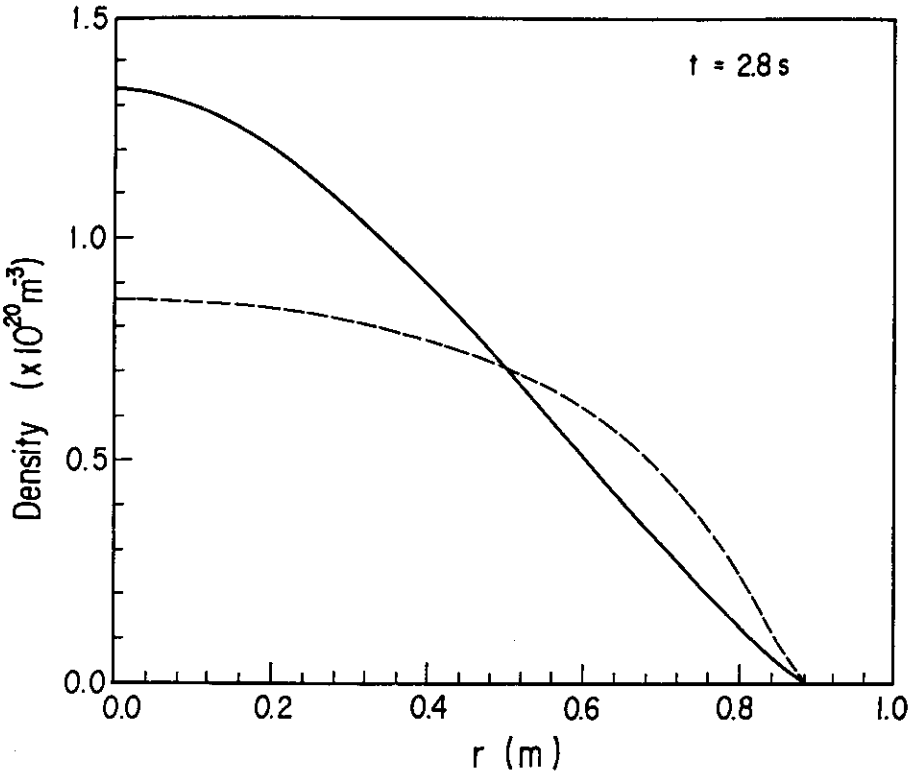


Fig. 12-c

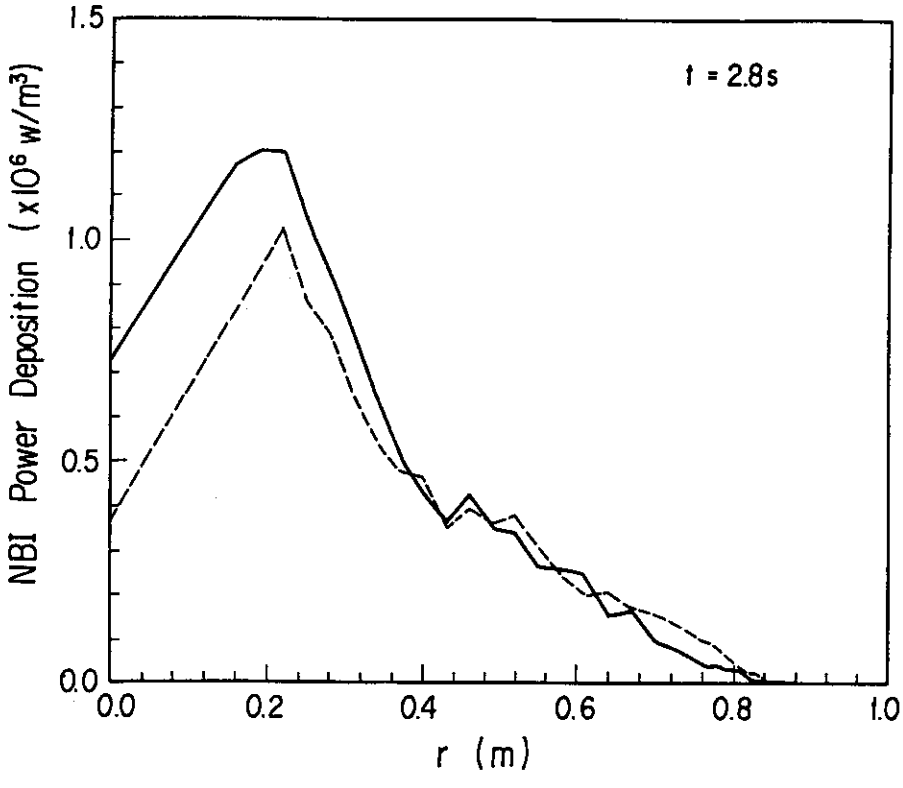


Fig. 12-d

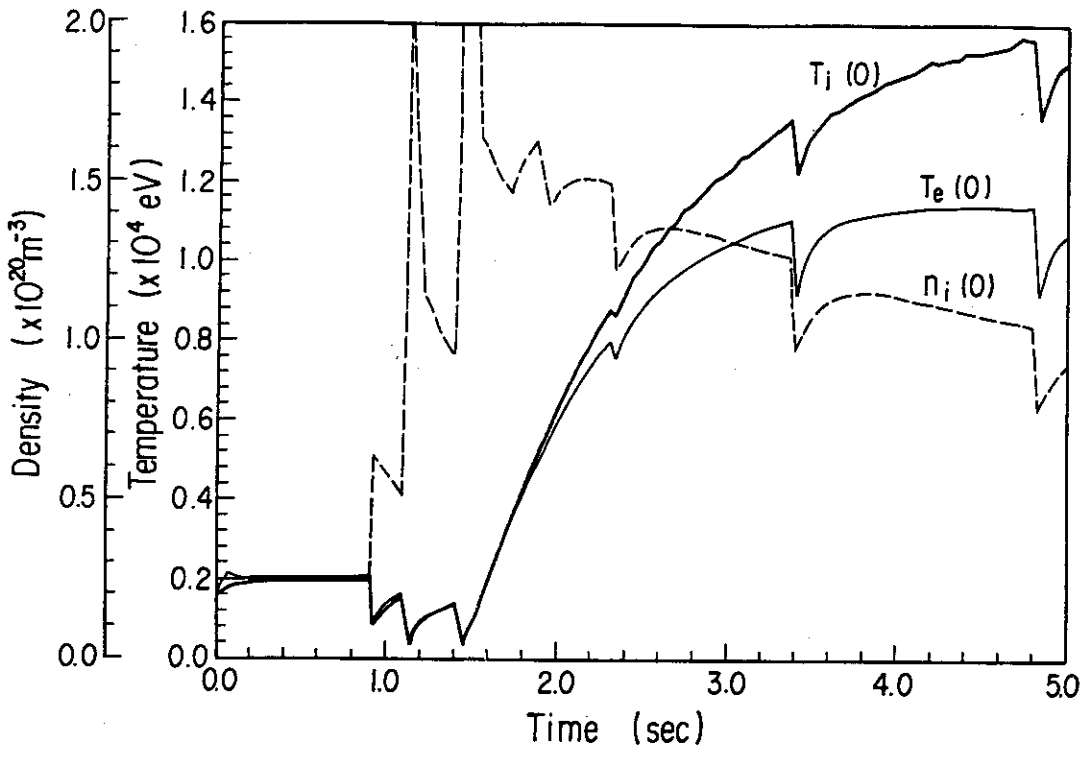


Fig.13 Time evolution of temperatures and density at the center in the case of the pellet injection.